

Measurement of the Two-Jet Differential Cross Section in $p\bar{p}$ Collisions at $\sqrt{s} = 1800$ GeV

T. Affolder,²³ H. Akimoto,⁴⁵ A. Akopian,³⁸ M. G. Albrow,¹¹ P. Amaral,⁸ S. R. Amendolia,³⁴ D. Amidei,²⁶ K. Anikeev,²⁴ J. Antos,¹ G. Apollinari,¹¹ T. Arisawa,⁴⁵ T. Asakawa,⁴³ W. Ashmanskas,⁸ F. Azfar,³¹ P. Azzi-Bacchetta,³² N. Bacchetta,³² M. W. Bailey,²⁸ S. Bailey,¹⁶ P. de Barbaro,³⁷ A. Barbaro-Galtieri,²³ V. E. Barnes,³⁶ B. A. Barnett,¹⁹ S. Baroiant,⁵ M. Barone,¹³ G. Bauer,²⁴ F. Bedeschi,³⁴ S. Belforte,⁴² W. H. Bell,¹⁵ G. Bellettini,³⁴ J. Bellinger,⁴⁶ D. Benjamin,¹⁰ J. Bensinger,⁴ A. Beretvas,¹¹ J. P. Berge,¹¹ J. Berryhill,⁸ B. Bevensee,³³ A. Bhatti,³⁸ M. Binkley,¹¹ D. Bisello,³² M. Bishai,¹¹ R. E. Blair,² C. Blocker,⁴ K. Bloom,²⁶ B. Blumenfeld,¹⁹ S. R. Blusk,³⁷ A. Bocci,³⁸ A. Bodek,³⁷ W. Bokhari,³³ G. Bolla,³⁶ Y. Bonushkin,⁶ D. Bortoletto,³⁶ J. Boudreau,³⁵ A. Brandl,²⁸ S. van den Brink,¹⁹ C. Bromberg,²⁷ M. Brozovic,¹⁰ N. Bruner,²⁸ E. Buckley-Geer,¹¹ J. Budagov,⁹ H. S. Budd,³⁷ K. Burkett,¹⁶ G. Busetto,³² A. Byon-Wagner,¹¹ K. L. Byrum,² P. Calafiura,²³ M. Campbell,²⁶ W. Carithers,²³ J. Carlson,²⁶ D. Carlsmith,⁴⁶ W. Caskey,⁵ J. Cassada,³⁷ A. Castro,³² D. Cauz,⁴² A. Cerri,³⁴ A. W. Chan,¹ P. S. Chang,¹ P. T. Chang,¹ J. Chapman,²⁶ C. Chen,³³ Y. C. Chen,¹ M. - T. Cheng,¹ M. Chertok,⁴⁰ G. Chiarelli,³⁴ I. Chirikov-Zorin,⁹ G. Chlachidze,⁹ F. Chlebana,¹¹ L. Christofek,¹⁸ M. L. Chu,¹ Y. S. Chung,³⁷ C. I. Ciobanu,²⁹ A. G. Clark,¹⁴ A. Connolly,²³ J. Conway,³⁹ M. Cordelli,¹³ J. Cranshaw,⁴¹ D. Cronin-Hennessy,¹⁰ R. Cropp,²⁵ R. Culbertson,¹¹ D. Dagenhart,⁴⁴ S. D'Auria,¹⁵ F. DeJongh,¹¹ S. Dell'Agnello,¹³ M. Dell'Orso,³⁴ L. Demortier,³⁸ M. Deninno,³ P. F. Derwent,¹¹ T. Devlin,³⁹ J. R. Dittmann,¹¹ S. Donati,³⁴ J. Done,⁴⁰ T. Dorigo,¹⁶ N. Eddy,¹⁸ K. Einsweiler,²³ J. E. Elias,¹¹ E. Engels, Jr.,³⁵ R. Erbacher,¹¹ D. Errede,¹⁸ S. Errede,¹⁸ Q. Fan,³⁷ R. G. Feild,⁴⁷ J. P. Fernandez,¹¹ C. Ferretti,³⁴ R. D. Field,¹² I. Fiori,³ B. Flaughner,¹¹ G. W. Foster,¹¹ M. Franklin,¹⁶ J. Freeman,¹¹ J. Friedman,²⁴ Y. Fukui,²² I. Furic,²⁴ S. Galeotti,³⁴ M. Gallinaro,³⁸ T. Gao,³³ M. Garcia-Sciveres,²³ A. F. Garfinkel,³⁶ P. Gatti,³² C. Gay,⁴⁷ D. W. Gerdes,²⁶ P. Giannetti,³⁴ P. Giromini,¹³ V. Glagolev,⁹ D. Glenzinski,¹¹ M. Gold,²⁸ J. Goldstein,¹¹ A. Gordon,¹⁶ I. Gorelov,²⁸ A. T. Goshaw,¹⁰ Y. Gotra,³⁵ K. Goulianos,³⁸ C. Green,³⁶ G. Grim,⁵ P. Gris,¹¹ L. Groer,³⁹ C. Grosso-Pilcher,⁸ M. Guenther,³⁶ G. Guillian,²⁶ J. Guimaraes da Costa,¹⁶ R. M. Haas,¹² C. Haber,²³ E. Hafen,²⁴ S. R. Hahn,¹¹ C. Hall,¹⁶ T. Handa,¹⁷ R. Handler,⁴⁶ W. Hao,⁴¹ F. Happacher,¹³ K. Hara,⁴³ A. D. Hardman,³⁶ R. M. Harris,¹¹ F. Hartmann,²⁰ K. Hatakeyama,³⁸ J. Hauser,⁶ J. Heinrich,³³ A. Heiss,²⁰ M. Herndon,¹⁹ C. Hill,⁵ K. D. Hoffman,³⁶ C. Holck,³³ R. Hollebeek,³³ L. Holloway,¹⁸ R. Hughes,²⁹ J. Huston,²⁷ J. Huth,¹⁶ H. Ikeda,⁴³ J. Incandela,¹¹ G. Introzzi,³⁴ J. Iwai,⁴⁵ Y. Iwata,¹⁷ E. James,²⁶ H. Jensen,¹¹ M. Jones,³³ U. Joshi,¹¹ H. Kambara,¹⁴

T. Kamon,⁴⁰ T. Kaneko,⁴³ K. Karr,⁴⁴ H. Kasha,⁴⁷ Y. Kato,³⁰ T. A. Keaffaber,³⁶
 K. Kelley,²⁴ M. Kelly,²⁶ R. D. Kennedy,¹¹ R. Kephart,¹¹ D. Khazins,¹⁰ T. Kikuchi,⁴³
 B. Kilminster,³⁷ B. J. Kim,²¹ D. H. Kim,²¹ H. S. Kim,¹⁸ M. J. Kim,²¹ S. H. Kim,⁴³
 Y. K. Kim,²³ M. Kirby,¹⁰ M. Kirk,⁴ L. Kirsch,⁴ S. Klimenko,¹² P. Koehn,²⁹
 A. Köngeter,²⁰ K. Kondo,⁴⁵ J. Konigsberg,¹² K. Kordas,²⁵ A. Korn,²⁴ A. Korytov,¹²
 E. Kovacs,² J. Kroll,³³ M. Kruse,³⁷ S. E. Kuhlmann,² K. Kurino,¹⁷ T. Kuwabara,⁴³
 A. T. Laasanen,³⁶ N. Lai,⁸ S. Lami,³⁸ S. Lammel,¹¹ J. I. Lamoureux,⁴ J. Lancaster,¹⁰
 M. Lancaster,²³ R. Lander,⁵ G. Latino,³⁴ T. LeCompte,² A. M. Lee IV,¹⁰ K. Lee,⁴¹
 S. Leone,³⁴ J. D. Lewis,¹¹ M. Lindgren,⁶ T. M. Liss,¹⁸ J. B. Liu,³⁷ Y. C. Liu,¹
 D. O. Litvintsev,⁸ O. Lobban,⁴¹ N. Lockyer,³³ J. Loken,³¹ M. Loreti,³² D. Lucchesi,³²
 P. Lukens,¹¹ S. Lusin,⁴⁶ L. Lyons,³¹ J. Lys,²³ R. Madrak,¹⁶ K. Maeshima,¹¹
 P. Maksimovic,¹⁶ L. Malferrari,³ M. Mangano,³⁴ M. Mariotti,³² G. Martignon,³²
 A. Martin,⁴⁷ J. A. J. Matthews,²⁸ J. Mayer,²⁵ P. Mazzanti,³ K. S. McFarland,³⁷
 P. McIntyre,⁴⁰ E. McKigney,³³ M. Menguzzato,³² A. Menzione,³⁴ C. Mesropian,³⁸
 A. Meyer,¹¹ T. Miao,¹¹ R. Miller,²⁷ J. S. Miller,²⁶ H. Minato,⁴³ S. Miscetti,¹³
 M. Mishina,²² G. Mitselmakher,¹² N. Moggi,³ E. Moore,²⁸ R. Moore,²⁶ Y. Morita,²²
 T. Moulik,²⁴ M. Mulhearn,²⁴ A. Mukherjee,¹¹ T. Muller,²⁰ A. Munar,³⁴ P. Murat,¹¹
 S. Murgia,²⁷ J. Nachtman,⁶ V. Nagaslaev,⁴¹ S. Nahn,⁴⁷ H. Nakada,⁴³ T. Nakaya,⁸
 I. Nakano,¹⁷ C. Nelson,¹¹ T. Nelson,¹¹ C. Neu,²⁹ D. Neuberger,²⁰ C. Newman-
 Holmes,¹¹ C.-Y. P. Ngan,²⁴ H. Niu,⁴ L. Nodulman,² A. Nomerotski,¹² S. H. Oh,¹⁰
 T. Ohmoto,¹⁷ T. Ohsugi,¹⁷ R. Oishi,⁴³ T. Okusawa,³⁰ J. Olsen,⁴⁶ W. Orejudos,²³
 C. Pagliarone,³⁴ F. Palmonari,³⁴ R. Paoletti,³⁴ V. Papadimitriou,⁴¹ S. P. Pappas,⁴⁷
 D. Partos,⁴ J. Patrick,¹¹ G. Pauletta,⁴² M. Paulini,^{(*) 23} C. Paus,²⁴ L. Pescara,³²
 T. J. Phillips,¹⁰ G. Piacentino,³⁴ K. T. Pitts,¹⁸ A. Pompos,³⁶ L. Pondrom,⁴⁶ G. Pope,³⁵
 M. Popovic,²⁵ F. Prokoshin,⁹ J. Proudfoot,² F. Ptohos,¹³ O. Pukhov,⁹ G. Punzi,³⁴
 K. Ragan,²⁵ A. Rakitine,²⁴ D. Reher,²³ A. Reichold,³¹ A. Ribon,³² W. Riegler,¹⁶
 F. Rimondi,³ L. Ristori,³⁴ M. Riveline,²⁵ W. J. Robertson,¹⁰ A. Robinson,²⁵
 T. Rodrigo,⁷ S. Rolli,⁴⁴ L. Rosenson,²⁴ R. Roser,¹¹ R. Rossin,³² A. Roy,²⁴ A. Safonov,³⁸
 R. St. Denis,¹⁵ W. K. Sakumoto,³⁷ D. Saltzberg,⁶ C. Sanchez,²⁹ A. Sansoni,¹³
 L. Santi,⁴² H. Sato,⁴³ P. Savard,²⁵ P. Schlabach,¹¹ E. E. Schmidt,¹¹ M. P. Schmidt,⁴⁷
 M. Schmitt,¹⁶ L. Scodellaro,³² A. Scott,⁶ A. Scribano,³⁴ S. Segler,¹¹ S. Seidel,²⁸
 Y. Seiya,⁴³ A. Semenov,⁹ F. Semeria,³ T. Shah,²⁴ M. D. Shapiro,²³ P. F. Shepard,³⁵
 T. Shibayama,⁴³ M. Shimojima,⁴³ M. Shochet,⁸ J. Siegrist,²³ A. Sill,⁴¹ P. Sinervo,²⁵
 P. Singh,¹⁸ A. J. Slaughter,⁴⁷ K. Sliwa,⁴⁴ C. Smith,¹⁹ F. D. Snider,¹¹ A. Solodsky,³⁸
 J. Spalding,¹¹ T. Speer,¹⁴ P. Sphicas,²⁴ F. Spinella,³⁴ M. Spiropulu,¹⁶ L. Spiegel,¹¹
 J. Steele,⁴⁶ A. Stefanini,³⁴ J. Strologas,¹⁸ F. Strumia,¹⁴ D. Stuart,¹¹ K. Sumorok,²⁴
 T. Suzuki,⁴³ T. Takano,³⁰ R. Takashima,¹⁷ K. Takikawa,⁴³ P. Tamburello,¹⁰
 M. Tanaka,⁴³ B. Tannenbaum,⁶ W. Taylor,²⁵ M. Tecchio,²⁶ R. Tesarek,¹¹ P. K. Teng,¹
 K. Terashi,³⁸ S. Tether,²⁴ A. S. Thompson,¹⁵ R. Thurman-Keup,² P. Tipton,³⁷
 S. Tkaczyk,¹¹ K. Tollefson,³⁷ A. Tollestrup,¹¹ H. Toyoda,³⁰ W. Trischuk,²⁵
 J. F. de Troconiz,¹⁶ J. Tseng,²⁴ N. Turini,³⁴ F. Ukegawa,⁴³ T. Vaiculis,³⁷ J. Valls,³⁹
 S. Vejcik III,¹¹ G. Velev,¹¹ R. Vidal,¹¹ R. Vilar,⁷ I. Volobouev,²³ D. Vucinic,²⁴
 R. G. Wagner,² R. L. Wagner,¹¹ J. Wahl,⁸ N. B. Wallace,³⁹ A. M. Walsh,³⁹ C. Wang,¹⁰

M. J. Wang,¹ T. Watanabe,⁴³ D. Waters,³¹ T. Watts,³⁹ R. Webb,⁴⁰ H. Wenzel,²⁰ W. C. Wester III,¹¹ A. B. Wicklund,² E. Wicklund,¹¹ T. Wilkes,⁵ H. H. Williams,³³ P. Wilson,¹¹ B. L. Winer,²⁹ D. Winn,²⁶ S. Wolbers,¹¹ D. Wolinski,²⁶ J. Wolinski,²⁷ S. Wolinski,²⁶ S. Worm,²⁸ X. Wu,¹⁴ J. Wyss,³⁴ A. Yagil,¹¹ W. Yao,²³ G. P. Yeh,¹¹ P. Yeh,¹ J. Yoh,¹¹ C. Yosef,²⁷ T. Yoshida,³⁰ I. Yu,²¹ S. Yu,³³ Z. Yu,⁴⁷ A. Zanetti,⁴² F. Zetti,²³ and S. Zucchelli³

(CDF Collaboration)

- ¹ *Institute of Physics, Academia Sinica, Taipei, Taiwan 11529, Republic of China*
² *Argonne National Laboratory, Argonne, Illinois 60439*
³ *Istituto Nazionale di Fisica Nucleare, University of Bologna, I-40127 Bologna, Italy*
⁴ *Brandeis University, Waltham, Massachusetts 02254*
⁵ *University of California at Davis, Davis, California 95616*
⁶ *University of California at Los Angeles, Los Angeles, California 90024*
⁷ *Instituto de Fisica de Cantabria, CSIC-University of Cantabria, 39005 Santander, Spain*
⁸ *Enrico Fermi Institute, University of Chicago, Chicago, Illinois 60637*
⁹ *Joint Institute for Nuclear Research, RU-141980 Dubna, Russia*
¹⁰ *Duke University, Durham, North Carolina 27708*
¹¹ *Fermi National Accelerator Laboratory, Batavia, Illinois 60510*
¹² *University of Florida, Gainesville, Florida 32611*
¹³ *Laboratori Nazionali di Frascati, Istituto Nazionale di Fisica Nucleare, I-00044 Frascati, Italy*
¹⁴ *University of Geneva, CH-1211 Geneva 4, Switzerland*
¹⁵ *Glasgow University, Glasgow G12 8QQ, United Kingdom*
¹⁶ *Harvard University, Cambridge, Massachusetts 02138*
¹⁷ *Hiroshima University, Higashi-Hiroshima 724, Japan*
¹⁸ *University of Illinois, Urbana, Illinois 61801*
¹⁹ *The Johns Hopkins University, Baltimore, Maryland 21218*
²⁰ *Institut für Experimentelle Kernphysik, Universität Karlsruhe, 76128 Karlsruhe, Germany*
²¹ *Center for High Energy Physics: Kyungpook National University, Taegu 702-701; Seoul National University, Seoul 151-742; and SungKyunKwan University, Suwon 440-746; Korea*
²² *High Energy Accelerator Research Organization (KEK), Tsukuba, Ibaraki 305, Japan*
²³ *Ernest Orlando Lawrence Berkeley National Laboratory, Berkeley, California 94720*
²⁴ *Massachusetts Institute of Technology, Cambridge, Massachusetts 02139*
²⁵ *Institute of Particle Physics: McGill University, Montreal H3A 2T8; and University of Toronto, Toronto M5S 1A7; Canada*
²⁶ *University of Michigan, Ann Arbor, Michigan 48109*
²⁷ *Michigan State University, East Lansing, Michigan 48824*
²⁸ *University of New Mexico, Albuquerque, New Mexico 87131*
²⁹ *The Ohio State University, Columbus, Ohio 43210*
³⁰ *Osaka City University, Osaka 588, Japan*
³¹ *University of Oxford, Oxford OX1 3RH, United Kingdom*

- ³² *Universita di Padova, Istituto Nazionale di Fisica Nucleare, Sezione di Padova, I-35131 Padova, Italy*
- ³³ *University of Pennsylvania, Philadelphia, Pennsylvania 19104*
- ³⁴ *Istituto Nazionale di Fisica Nucleare, University and Scuola Normale Superiore of Pisa, I-56100 Pisa, Italy*
- ³⁵ *University of Pittsburgh, Pittsburgh, Pennsylvania 15260*
- ³⁶ *Purdue University, West Lafayette, Indiana 47907*
- ³⁷ *University of Rochester, Rochester, New York 14627*
- ³⁸ *Rockefeller University, New York, New York 10021*
- ³⁹ *Rutgers University, Piscataway, New Jersey 08855*
- ⁴⁰ *Texas A&M University, College Station, Texas 77843*
- ⁴¹ *Texas Tech University, Lubbock, Texas 79409*
- ⁴² *Istituto Nazionale di Fisica Nucleare, University of Trieste/ Udine, Italy*
- ⁴³ *University of Tsukuba, Tsukuba, Ibaraki 305, Japan*
- ⁴⁴ *Tufts University, Medford, Massachusetts 02155*
- ⁴⁵ *Waseda University, Tokyo 169, Japan*
- ⁴⁶ *University of Wisconsin, Madison, Wisconsin 53706*
- ⁴⁷ *Yale University, New Haven, Connecticut 06520*
- (*) *Now at Carnegie Mellon University, Pittsburgh, Pennsylvania 15213*

Abstract

A measurement is presented of the two-jet differential cross section, $d^3\sigma/dE_T d\eta_1 d\eta_2$, at center of mass energy $\sqrt{s} = 1800$ GeV in $p\bar{p}$ collisions. The results are based on an integrated luminosity of 86 pb^{-1} collected during 1994-1995 by the CDF collaboration at the Fermilab Tevatron collider. The differential cross section is measured as a function of the transverse energy, E_T , of a jet in the pseudorapidity region $0.1 < |\eta_1| < 0.7$ for four different pseudorapidity bins of a second jet restricted to $0.1 < |\eta_2| < 3.0$. The results are compared with next-to-leading order QCD calculations determined using the CTEQ4 and MRST sets of parton distribution functions. None of the sets examined in this analysis provides a good description of the data.

PACS numbers: 13.85.Rm, 12.38.Qk

Jet production in proton-antiproton collisions results predominantly from hard interactions between two initial state partons. Theoretical developments in both perturbative next-to-leading order (NLO) and parton shower Monte Carlo calculations permit calculation of many QCD jet processes with theoretical uncertainties small enough to allow detailed comparison with measured distributions [1]. In this paper, we present a measurement of the dijet differential cross section that provides more precise information about the initial state partons than has been probed by previous CDF measurements of inclusive jet transverse energy [2], total transverse energy [3], and dijet mass [4]. All previous measurements showed an excess of events at high jet energies when compared to the QCD prediction based on standard sets of parton distribution functions (PDFs). One explanation for this excess is a larger than expected number of high momentum partons, particularly gluons, in the proton [5, 6]. While those measurements provide cross sections averaged over a wide range in their variable, in this analysis we reduce the region over which averages are taken by measuring the cross section for four separate ranges. This provides more detailed information about the cross section shape. Previous measurements of the dijet differential cross section have been performed by the CDF [7] and DØ [8] collaborations with smaller data samples. The present measurement places new constraints on the parton distributions of the proton.

Jet production rates are usually expressed in terms of the transverse energy, E_T , and pseudorapidity, η , of the jets, where η is related to the polar angle θ relative to the proton beam line by $\eta \equiv -\ln[\tan(\theta/2)]$. At leading order in QCD, the proton,

p , and anti-proton, \bar{p} , momentum fractions, x_1 and x_2 , carried by the two colliding partons can be expressed as

$$x_1 = \frac{E_T}{\sqrt{s}}(e^{\eta_1} + e^{\eta_2}), \quad x_2 = \frac{E_T}{\sqrt{s}}(e^{-\eta_1} + e^{-\eta_2}). \quad (1)$$

Here η_1 and η_2 are the pseudorapidities of the two jets, \sqrt{s} is the center of mass energy of the colliding hadrons and E_T is the transverse energy of the leading jet. For a fixed E_T and η_1 , one can probe higher x values by selecting events in which the second jet has a larger η_2 value. For a given x we have four measurements at what are effectively different values of Q^2 the square of the four-momentum transferred in the interaction, calculated by

$$Q^2 = 2E_T^2 \cosh^2 \eta^* (1 - \tanh \eta^*), \quad \eta^* = \frac{1}{2}(\eta_1 - \eta_2). \quad (2)$$

The four distributions in this analysis allow us to measure the cross section on a surface in the x - Q^2 phase space whose shape is sensitive to the predictions of different PDFs.

The constraint on the parton distributions at high x comes mainly from prompt photon production in pp or pA collisions from WA70 [9] and the E706 [10] experiments and inclusive jet data from the Tevatron [2]. The data do not constrain the parton distributions very well at high x . The higher statistics of this measurement together with the multiple cross section measurements at different Q^2 for approximately the same x provide a precise set of data which can be used to determine improved sets of PDFs. The current measurement, based on data of an integrated luminosity of

86 pb⁻¹ from 1.8 TeV $p\bar{p}$ collisions taken during the 1994-1995 Fermilab Tevatron collider run, covers the range $0.05 \lesssim x_1 \lesssim 0.8$.

The CDF detector is described in detail in [11]. In this analysis we utilize the central, plug, and forward calorimeters. The central calorimeter covers the pseudorapidity range $|\eta| < 1.1$. It is segmented into projective towers of size $\Delta\eta \times \Delta\phi = 0.1 \times 0.26$, where ϕ is the azimuthal angle in radians. The plug ($1.1 < |\eta| < 2.4$) and forward ($2.4 < |\eta| < 4.2$) calorimeters are segmented by approximately 5° in ϕ and 0.1 in η . The event vertex is resolved to within 1 mm along the z axis, using time projection chambers surrounding the beam pipe.

A cone algorithm with cone radius $R \equiv \sqrt{(\Delta\phi)^2 + (\Delta\eta)^2} = 0.7$ is used to identify jets [12]. Transverse energy is defined as $E_T = E \sin\theta$, where E is the scalar sum of energy deposited in the calorimeter towers within the cone and θ is the angle formed by the event vertex, the beam direction, and the cone center. Our data sample consists of events collected by on-line identification of at least one jet with transverse energy above trigger thresholds of 20, 50, 70, and 100 GeV at integrated luminosities of 0.091, 2.2, 11, and 86 pb⁻¹, respectively. The bin widths in E_T were chosen to be larger than the measurement resolution on E_T and to ensure sufficient statistics in the bins.

In this analysis we use events with at least two jets of $E_T > 10$ GeV of uncorrected energy. We consider events in which the E_T -weighted centroid of at least one of the two highest E_T jets is in the range $0.1 < |\eta| < 0.7$. This “leading” jet is required to deposit more than 40 GeV E_T , prior to corrections, in the central calorimeter.

In addition, the centroid of the second leading jet is required to be in the region $0.1 < |\eta| < 3.0$, and the primary event vertex must be located within ± 60 cm of the nominal interaction point. Poorly measured events and background from cosmic rays, beam halo, and detector noise are removed by requiring that total energy recorded by the detector be less than 2000 GeV and $\cancel{E}_T/\sqrt{\Sigma E_T} < 6\sqrt{\text{GeV}}$, where \cancel{E}_T is the missing transverse energy and ΣE_T is the scalar sum of the total transverse energy.

In this analysis, we evaluate the E_T spectrum of the leading jet for the following four η bins of the second leading jet in the event:

$$\begin{aligned} 0.1 < |\eta_2| < 0.7, & & 0.7 < |\eta_2| < 1.4, \\ 1.4 < |\eta_2| < 2.1, & & 2.1 < |\eta_2| < 3.0. \end{aligned}$$

The η_2 ranges were chosen to place regions of reduced response (due to gaps between detectors) within single bins while at the same time maintaining a sufficient number of events in the bins. Both jets are included in the distribution for the $0.1 < |\eta_2| < 0.7$ bin if each satisfies the requirement $0.1 < |\eta| < 0.7$ and $E_T > 40$ GeV.

Since the calorimetric response varies as a function of η , we determine the trigger response separately for each η_2 bin. The trigger efficiency was measured using overlapping E_T regions for the different trigger thresholds. For the 20 GeV trigger threshold, for which no lower E_T trigger was available, the second jet in the event was used to determine the trigger efficiency. For the four trigger thresholds, the trigger efficiency was found to be greater than 90% for jets of E_T greater than 40, 82, 105, and 130 GeV.

The measured jet E_T must be corrected for calorimeter non-linearity and loss of

energy in the gaps between calorimeters. In addition, the measured jet E_T spectrum must be corrected for the smearing effect caused by the resolution in the measured jet E_T . We simultaneously correct all these effects with the procedure used in our previous measurement of the inclusive jet E_T spectrum [2]. For the central η bin ($0.1 < |\eta_1| < 0.7$) at 40 GeV, the correction to the measured E_T is approximately 4%, while the correction to the measured cross section is about 19%. The correction to the cross section increases to 70% for the bin $2.1 < |\eta_1| < 3.0$. The corrected cross section values are given in Tables 1 and 2 and plotted in Figure 1.

The systematic error on the measurement of the jet cross section is dominated by the uncertainty in the measurement of the jet E_T magnified by the steep slope of the E_T spectrum. Although the same sources of uncertainty contribute to the cross section of each E_T bin, the uncertainty depends on the local slope of the E_T spectrum. The systematic uncertainties were evaluated as in References [2] and [13]. The uncertainties include: charged hadron response at high p_T (h pt); calorimeter response to low- p_T hadrons (l pt); ± 1 % on the jet energy of the absolute calibration of the calorimeter (esc); jet fragmentation functions used in the simulation (frag); $\pm 30\%$ on the underlying event energy in the jet cone (uevt); detector response to electrons and photons (e/ph); and modeling of the detector jet energy resolution (cres). The resolution on the measured η causes events to migrate between adjacent bins. In the highest η bin, the gap between the plug and forward calorimeters results in decreased η resolution and has the effect that more events migrate out of the bin than into it. To compensate for this effect, we have applied an E_T -dependent

$0.1 < \eta_2 < 0.7$				$0.7 < \eta_2 < 1.4$			
$\langle E_T \rangle$	$d\sigma/dE_T$	stat	sys	$\langle E_T \rangle$	$d\sigma/dE_T$	stat	sys
(GeV)	(nb/GeV)	%	%	(GeV)	(nb/GeV)	%	%
44.0	1.23×10^1	1.3	19.5	43.1	1.29×10^1	1.3	21.5
50.0	6.48×10^0	1.7	18.4	49.5	6.41×10^0	1.7	19.6
58.9	2.78×10^0	1.6	17.2	58.5	2.65×10^0	1.6	17.8
75.5	7.54×10^{-1}	2.4	15.9	75.2	6.73×10^{-1}	2.5	16.2
94.3	2.22×10^{-1}	1.2	15.3	94.0	1.87×10^{-1}	1.3	15.7
106.6	1.10×10^{-1}	1.5	14.6	106.2	9.36×10^{-2}	1.6	15.1
119.5	5.83×10^{-2}	1.1	14.6	119.1	4.54×10^{-2}	1.2	15.2
132.5	3.13×10^{-2}	1.2	14.5	132.0	2.41×10^{-2}	1.3	15.4
150.8	1.42×10^{-2}	0.6	14.8	150.0	1.03×10^{-2}	0.6	16.0
174.4	5.53×10^{-3}	0.8	15.2	173.2	3.85×10^{-3}	0.9	16.9
209.4	1.67×10^{-3}	1.1	16.2	206.9	9.92×10^{-4}	1.4	18.9
264.1	3.10×10^{-4}	2.5	18.3	260.5	1.33×10^{-4}	3.9	22.9
318.2	6.06×10^{-5}	5.9	20.7	313.7	1.98×10^{-5}	10.4	27.7
382.4	1.14×10^{-5}	10.9	24.5	373.9	3.37×10^{-6}	21.3	34.6

Table 1: The measured dijet differential cross sections for $0.1 < |\eta_2| < 0.7$ and $0.7 < |\eta_2| < 1.4$. The differential cross section is given for the average E_T of the bin. The statistical and systematic errors are shown as a percentage of the central value.

$1.4 < \eta_2 < 2.1$				$2.1 < \eta_2 < 3.0$			
$\langle E_T \rangle$	$d\sigma/dE_T$	stat	sys	$\langle E_T \rangle$	$d\sigma/dE_T$	stat	sys
(GeV)	(nb/GeV)	%	%	(GeV)	(nb/GeV)	%	%
42.1	1.14×10^1	1.4	22.6	40.9	5.81×10^0	2.0	27.3
48.9	5.04×10^0	1.9	20.8	47.5	2.39×10^0	2.7	25.1
58.0	1.99×10^0	1.9	19.4	56.2	7.85×10^{-1}	3.0	23.7
74.3	4.72×10^{-1}	3.0	18.4	71.7	1.40×10^{-1}	5.8	23.5
93.0	1.08×10^{-1}	1.7	18.5	90.4	1.93×10^{-2}	4.3	25.0
104.9	4.83×10^{-2}	2.3	18.4	101.8	7.47×10^{-3}	6.1	26.1
117.5	2.21×10^{-2}	1.8	19.0	114.2	2.28×10^{-3}	5.9	27.9
130.0	1.03×10^{-2}	2.1	19.7	126.0	8.13×10^{-4}	8.3	29.8
147.4	3.48×10^{-3}	1.2	21.0	142.5	1.89×10^{-4}	5.5	32.7
169.8	9.59×10^{-4}	2.0	22.9	163.7	2.39×10^{-5}	14.7	36.4
200.8	1.88×10^{-4}	3.6	26.3	191.4	3.64×10^{-6}	33.3	40.4
252.7	1.06×10^{-5}	15.8	33.3				

Table 2: The measured dijet differential cross sections for $1.4 < |\eta_2| < 2.1$ and $2.1 < |\eta_2| < 3.0$. The differential cross section is given for the average E_T of the bin. The statistical and systematic errors are shown as a percentage of the central value.

correction which is less than 8% in all bins. The effect was studied by breaking it into two components, the resolution on the measured η (η res) and a systematic shift in the reconstructed η (η sh). It is included in the systematic error by looking at the result on the cross section when doubling and halving the correction. Bins for which events were collected using triggers with uncorrected energy greater than 20 GeV (J20), 50 GeV (J50) and 70 GeV (J70) were assigned 4, 2 and 2 percent errors respectively, associated with prescaling. An overall luminosity uncertainty (norm) of 4 percent is added in quadrature with these. The sources of systematic errors are listed in Tables 3 through 6 as percentages of the central E_T value for each E_T and η bin. In general the percent error increases as η_2 increases.

In Figure 2, the difference between the fully corrected two-jet differential cross section and the predicted cross section is divided by the predicted cross section and plotted as a function of the leading jet E_T for the four η ranges of the second jet. The theory predictions were calculated using the NLO calculation of the JETRAD program [14] with the PDFs indicated. The calculations use a renormalization scale $\mu = E_T^{max}/2$ with $R_{sep} = 1.3$, where R_{sep} is a measure of the maximum separation between the cones of two jets that are merged into one. The error bars represent the statistical errors, while the shaded bands represent one standard deviation of the systematic error, which is correlated for all the different E_T values. The data are compared to the predicted cross section obtained using the PDF set CTEQ4M [5]. The solid curve shows the expected results when using CTEQ4HJ [5], and the dashed curves show the results when using the PDF set MRST [15].

$\langle E_T \rangle$	e/ph	uevt	frag	esc	cres	l pt	h pt	η sh	η res	norm	J20	J50	J70	tot
43.9	2.5	12.7	7.9	4.1	4.9	7.3	2.6	2.5	0.4	4.0	4.0	2.0	2.0	19.5
50.0	2.6	11.1	8.0	4.0	4.5	7.3	2.9	2.5	0.4	4.0	4.0	2.0	2.0	18.4
58.9	2.6	9.1	8.1	4.0	4.0	7.1	3.4	2.5	0.4	4.0	4.0	2.0	2.0	17.2
75.5	2.8	6.6	8.1	4.1	3.2	6.7	4.3	2.5	0.4	4.0	4.0	2.0	2.0	15.9
94.3	2.9	5.1	7.9	4.3	2.6	6.2	5.3	2.4	0.4	4.0	4.0	2.0	2.0	15.3
106.6	2.9	4.4	7.7	4.5	2.3	5.9	5.9	2.4	0.4	4.0	0.0	2.0	2.0	14.6
119.5	3.0	4.0	7.6	4.6	2.1	5.5	6.6	2.4	0.4	4.0	0.0	2.0	2.0	14.6
132.5	3.1	3.6	7.4	4.8	2.0	5.2	7.3	2.3	0.4	4.0	0.0	0.0	2.0	14.5
150.8	3.2	3.3	7.3	5.1	2.0	4.8	8.1	2.3	0.4	4.0	0.0	0.0	2.0	14.8
174.4	3.3	3.1	7.2	5.4	2.1	4.4	9.1	2.2	0.4	4.0	0.0	0.0	0.0	15.2
209.4	3.6	2.9	7.4	5.9	2.4	4.0	10.5	2.0	0.4	4.0	0.0	0.0	0.0	16.2
264.1	4.2	2.7	8.3	6.7	2.9	4.0	12.3	1.7	0.3	4.0	0.0	0.0	0.0	18.3
318.2	4.9	2.5	10.0	7.4	3.5	4.8	13.8	1.2	0.3	4.0	0.0	0.0	0.0	20.7
382.4	5.8	2.3	13.4	8.2	5.0	6.8	15.0	0.6	0.9	4.0	0.0	0.0	0.0	24.5

Table 3: The systematic errors for the $0.1 < \eta_2 < 0.7$ bin given as a percentage of the central value. The E_T values are specified at the bin average. A reference to the sources of systematic errors is given in the text.

$\langle E_T \rangle$	e/ph	uevt	frag	esc	cres	l pt	h pt	η sh	η res	norm	J20	J50	J70	tot
43.1	2.6	15.0	8.3	4.2	6.1	7.7	2.7	0.6	0.3	4.0	4.0	2.0	2.0	21.5
49.5	2.6	12.3	8.5	4.1	5.4	7.6	3.1	0.5	0.3	4.0	4.0	2.0	2.0	19.6
58.5	2.7	9.5	8.6	4.1	4.6	7.4	3.6	0.5	0.3	4.0	4.0	2.0	2.0	17.8
75.2	2.8	6.6	8.5	4.1	3.4	7.0	4.6	0.5	0.3	4.0	4.0	2.0	2.0	16.2
94.0	3.0	5.0	8.4	4.3	2.6	6.5	5.7	0.4	0.2	4.0	4.0	2.0	2.0	15.7
106.2	3.1	4.5	8.3	4.5	2.3	6.2	6.4	0.5	0.2	4.0	0.0	2.0	2.0	15.1
119.1	3.2	4.1	8.2	4.8	2.2	5.9	7.2	0.5	0.2	4.0	0.0	2.0	2.0	15.2
131.9	3.3	3.9	8.1	5.1	2.1	5.6	7.9	0.5	0.2	4.0	0.0	0.0	2.0	15.4
150.0	3.5	3.8	8.1	5.5	2.3	5.2	9.0	0.6	0.3	4.0	0.0	0.0	2.0	16.0
173.2	3.8	3.7	8.2	6.1	2.6	4.9	10.3	0.7	0.3	4.0	0.0	0.0	0.0	16.9
206.9	4.2	3.6	8.7	7.1	3.3	4.7	12.2	1.0	0.5	4.0	0.0	0.0	0.0	18.9
260.5	5.1	3.5	10.4	8.9	4.5	5.0	15.2	1.7	1.1	4.0	0.0	0.0	0.0	22.9
313.7	6.0	3.4	13.2	10.9	5.4	6.0	18.2	2.6	2.3	4.0	0.0	0.0	0.0	27.7
373.9	7.1	3.2	17.9	13.5	6.7	8.1	21.7	3.9	4.7	4.0	0.0	0.0	0.0	34.6

Table 4: The systematic errors for the $0.7 < \eta_2 < 1.4$ bin given as a percentage of the central value. The E_T values are specified at the bin average. A reference to the sources of systematic errors is given in the text.

$\langle E_T \rangle$	e/ph	uevt	frag	esc	cres	l pt	h pt	η sh	η res	norm	J20	J50	J70	tot
42.1	2.8	15.7	8.5	4.3	6.6	7.8	2.8	3.6	0.5	4.0	4.0	2.0	2.0	22.6
48.9	2.9	12.8	8.9	4.6	5.8	8.0	3.1	3.4	0.5	4.0	4.0	2.0	2.0	20.8
58.0	3.0	10.2	9.3	4.8	5.0	8.0	3.7	3.2	0.4	4.0	4.0	2.0	2.0	19.4
74.3	3.2	7.6	9.6	5.1	4.0	7.9	5.1	3.0	0.3	4.0	4.0	2.0	2.0	18.4
93.0	3.5	6.3	9.8	5.4	3.6	7.5	6.9	2.6	0.2	4.0	4.0	2.0	2.0	18.5
104.9	3.7	5.8	10.0	5.6	3.5	7.3	8.0	2.4	0.2	4.0	0.0	2.0	2.0	18.4
117.5	4.0	5.6	10.1	5.9	3.6	7.0	9.3	2.2	0.1	4.0	0.0	2.0	2.0	19.0
130.0	4.2	5.4	10.3	6.3	3.8	6.9	10.5	2.1	0.1	4.0	0.0	0.0	2.0	19.7
147.4	4.6	5.2	10.6	6.9	4.3	6.7	12.1	1.8	0.5	4.0	0.0	0.0	2.0	21.0
169.7	5.1	5.1	11.2	7.8	5.0	6.5	14.1	1.6	1.2	4.0	0.0	0.0	0.0	22.9
200.8	5.8	4.9	12.4	9.5	6.1	6.7	16.8	1.2	2.7	4.0	0.0	0.0	0.0	26.2
252.7	7.3	4.6	15.4	13.2	8.5	7.8	20.8	0.8	6.7	4.0	0.0	0.0	0.0	33.3

Table 5: The systematic errors for the $1.4 < \eta_2 < 2.1$ bin given as a percentage. The E_T values are specified at the bin average. A reference to the sources of systematic errors is given in the text.

$\langle E_T \rangle$	e/ph	uevt	frag	esc	cres	l pt	h pt	η sh	η res	norm	J20	J50	J70	tot
40.9	3.1	19.9	9.7	4.9	9.0	9.0	3.2	3.1	0.5	4.0	4.0	2.0	2.0	27.3
47.5	3.3	16.3	10.3	5.3	8.3	9.2	3.9	2.9	0.4	4.0	4.0	2.0	2.0	25.1
56.2	3.6	13.4	10.9	5.7	7.5	9.5	4.8	2.7	0.2	4.0	4.0	2.0	2.0	23.7
71.7	4.1	10.8	12.1	6.4	6.5	9.8	6.8	2.5	0.2	4.0	4.0	2.0	2.0	23.5
90.4	4.8	9.7	13.3	7.4	6.5	10.0	9.3	2.9	0.7	4.0	4.0	2.0	2.0	25.0
101.8	5.2	9.4	13.9	8.0	7.0	10.1	11.0	3.3	1.0	4.0	0.0	2.0	2.0	26.1
114.2	5.7	9.2	14.5	8.7	8.0	10.1	12.9	4.0	1.3	4.0	0.0	2.0	2.0	27.9
126.0	6.1	9.1	15.1	9.4	9.3	10.1	14.7	4.9	1.7	4.0	0.0	0.0	2.0	29.8
142.4	6.8	9.0	15.8	10.3	11.0	10.0	17.4	6.4	2.2	4.0	0.0	0.0	2.0	32.7
163.6	7.7	8.9	16.5	11.5	11.9	9.7	20.9	8.9	2.9	4.0	0.0	0.0	0.0	36.4
191.4	8.8	8.8	17.3	13.0	7.3	9.3	25.8	13.2	4.0	4.0	0.0	0.0	0.0	40.4

Table 6: The systematic errors for the $2.1 < \eta_2 < 3.0$ bin given as a percentage. The E_T values are specified at the bin average. A reference to the sources of systematic errors is given in the text.

The observed excess of events at high E_T values in the inclusive jet cross section measurement may be explained within the framework of conventional QCD by exploiting the relatively weak restriction on the gluon density at high x [6]. The CTEQ4 PDFs use a more flexible parameterization of the gluon density at high x than is present in other sets. The CTEQ4 set of PDFs include the inclusive jet data from the Tevatron. The CTEQ4HJ PDF gives a higher weight to the inclusive jet data while still maintaining agreement with the other data sets used in the fit.

The MRST set of PDFs is based in a wide range of deep inelastic scattering data and has an improved treatment of heavy flavors and prompt photon production than do previous MRST sets. The main constraint upon the gluon at high x comes from prompt photon production from the WA70 [9] and E706 [10] data. The set MRST(g \uparrow) was derived assuming that there is no initial state partonic transverse momentum ($\langle k_T \rangle = 0$); this does not lead to a good fit for the prompt photon data from the E706 experiment. The set labelled MRST(g \downarrow) was derived by allowing non-zero $\langle k_T \rangle$ while maintaining reasonable agreement with the WA70 data. The MRST(g \downarrow) set has $\langle k_T \rangle = 0.64$ GeV. These two sets represent the extreme values of $\langle k_T \rangle$ that yield reasonable agreement with the data used in the fit. The set labelled MRST represents the preferred set from the global analysis and has $\langle k_T \rangle = 0.4$ GeV.

The covariance matrix for the dijet cross section is

$$V_{ij} = \delta_{ij}\sigma_i^2(stat) + \sum_{k=1}^{13}\sigma_i(sys_k)\sigma_j(sys_k),$$

where $\delta_{ij} = 1(0)$ for $i = j(i \neq j)$ $\sigma_i(stat)$ is the statistical uncertainty in bin i and

$\sigma_i(sy s_k)$ is the systematic uncertainty, k , on bin i . The sum is over the 13 sources of systematic errors listed above and over all the E_T bins in each of the four η bins. We calculate the χ^2 from $\chi^2 = \Sigma_{ij} \Delta_i (V^{-1})_{ij} \Delta_j$, where Δ_i is the difference between the data and theoretical prediction for bin i . The average of the upper and lower errors is used when calculating the χ^2 . The χ^2/dof values for different PDFs are presented in Table 7. Although the cross sections predicted by the MRST PDFs are lower than the data by 20%, they have similar χ^2 values to those predicted with CTEQ4M. This is because the systematic errors allow a correlated shift in the data which makes only a small contribution to the total χ^2 . Predictions whose shape matches that of a correlated systematic error will give reasonable χ^2 values provided that the normalization between the data and prediction are within a few standard deviations. The probability of describing the data with the PDFs used in this analysis is less than 1% in all cases.

PDF	χ^2/dof	PDF	χ^2/dof
MRST	2.68	CTEQ4HJ	2.43
MRST(g \uparrow)	3.63	CTEQ4M	2.88
MRST(g \downarrow)	4.49		

Table 7: The χ^2/dof between the data and the prediction of Giele, et al., for different PDFs. The fit to the data has 51 degrees of freedom.

In summary, we have measured the differential cross section for dijet production in $p\bar{p}$ collisions with one jet restricted to the pseudorapidity region $0.1 < |\eta_1| < 0.7$ for

four different pseudorapidity bins of a second jet restricted within $0.1 < |\eta_2| < 3.0$. By allowing the pseudorapidity of the second jet to vary through $0.1 < |\eta| < 3.0$, we are able to map out the cross section over the available kinematic phase space and provide a differential cross section that more tightly constrains the parton distributions of the proton than in measurements previously reported by us. The measurement provides more precise information about the parton distributions of the proton in the high x region, an area which is not well constrained, and will provide useful input to QCD global fits. The resulting improved sets of PDFs will help to further enhance our knowledge of the structure functions of the proton.

We thank the Fermilab staff and the technical staffs of the participating institutions for their vital contributions. This work was supported by the U.S. Department of Energy and National Science Foundation; the Italian Istituto Nazionale di Fisica Nucleare; the Ministry of Education, Science, Sports and Culture of Japan; the Natural Sciences and Engineering Research Council of Canada; the National Science Council of the Republic of China; the Swiss National Science Foundation; the A. P. Sloan Foundation; the Bundesministerium fuer Bildung und Forschung, Germany; and the Korea Science and Engineering Foundation.

References

- [1] S. Ellis, Z. Kunszt and D. Soper, Phys. Rev. Lett. **64** 2121 (1990); W.T. Giele, E.W.N. Glover and D.A. Kosower, Nucl. Phys. **B403**, 633 (1993).

- [2] CDF Collaboration, F. Abe *et al.*, Phys. Rev. Lett. **77**, 438 (1996).
- [3] CDF Collaboration, F. Abe *et al.*, Phys. Rev. Lett. **80**, 3461 (1998).
- [4] CDF Collaboration. T. Affolder *et al.*, Phys. Rev. D **61**, 091101 (2000).
- [5] H.L. Lai *et al.*, Phys. Rev. D **55**, 1280 (1997).
- [6] CTEQ Collaboration, J. Huston *et al.*, Phys. Rev. Lett. **77**, 44 (1996).
- [7] CDF Collaboration, F. Abe *et al.*, Phys. Rev. Lett. **64**, 157 (1990).
- [8] DØ Collaboration, T. Asakawa *et al.*, Proceedings of Hadron Collider Phys. Workshop XIII Jan. 14-20, 1999, Bombay, India.
- [9] WA70 Collaboration, M. Bonesini *et al.*, Z. Phys. **C38**, 244 (1994).
- [10] E706 Collaboration, L. Apanasevich *et al.*, Phys. Rev. Lett., **81**, 2642 (1998).
- [11] CDF Collaboration, F. Abe *et al.*, Nucl. Instrum. Methods **A271**, 387 (1988).
- [12] CDF Collaboration, F. Abe *et al.*, Phys. Rev. D**45**, 1448 (1992).
- [13] CDF Collaboration, F. Abe *et al.*, Phys. Rev. Lett. **70**, 1376 (1993).
- [14] W.T. Giele, E.W.N. Glover and D.A. Kosower, Phys. Rev. Lett., **73**, 2019 (1994).
- [15] A.D. Martin, *et al.*, Eur. Phys. J. C**4**, 463 (1998).

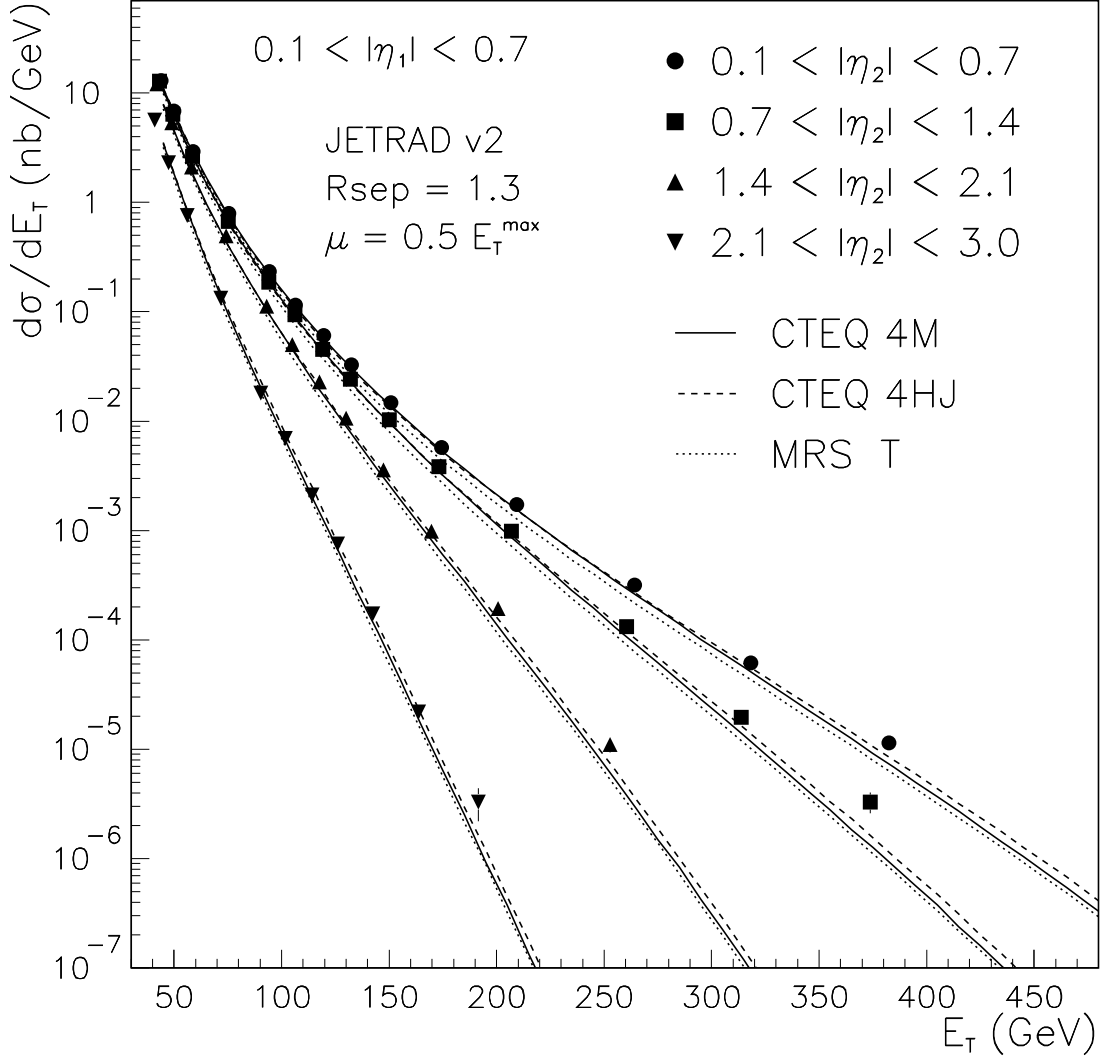


Figure 1: The differential cross section for dijet events as a function of transverse energy, E_T , and pseudorapidity, η , of one jet, for 4 ranges in the pseudorapidity of the other jet. The results are compared with QCD predictions using different parton distribution functions.

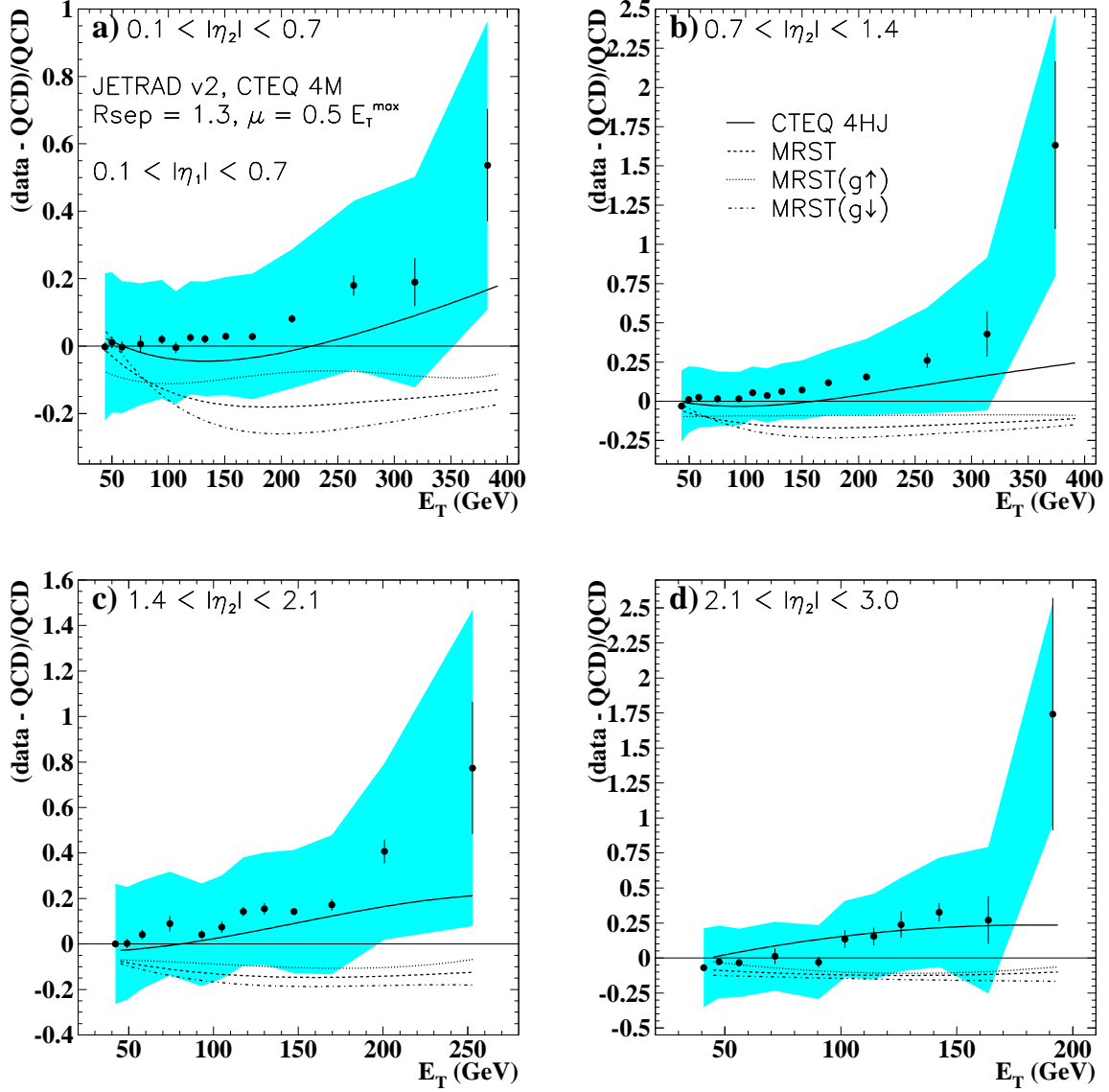


Figure 2: The differential cross section for dijet events as a function of transverse energy, E_T , and pseudorapidity, η , of the leading jet, for four ranges in the pseudorapidity of the second leading jet. The results are compared with QCD predictions using different parton distribution functions. The statistical error is represented by the error bars while the correlated systematic error is shown as the shaded band.